

The Impact of Convective Flow on Thermal Diffusion Cloud Chamber Operation[†]

Frank Ferguson[‡] and Richard H. Heist^{*§}

Department of Chemistry, Catholic University of America, Washington, D.C. 20064 and Department of Chemical Engineering, Manhattan College, Riverdale, New York 10471-4098

Received: May 15, 2001; In Final Form: August 7, 2001

We report here new results that further elucidate the role of buoyancy-driven convective flows in determining the distribution of vapor mole fraction and temperature in the thermal diffusion cloud chamber. A two-dimensional model describing both diffusion and convection in the presence of chamber sidewalls is presented. The model equations are used to analyze 1-butanol and 1-pentanol nucleation data obtained earlier. The results of the investigation show that convective flow is nearly always present and, in the cases considered here, result in a reduction in the value of the calculated critical supersaturation (as compared to the one-dimensional case). The dependence of critical supersaturation with total pressure reported earlier is smaller but is not eliminated.

Introduction

The thermal diffusion cloud chamber (TDCC) has been used extensively for nucleation research for more than four decades. It is an important complement to expansion- and flow-based devices, for example, expansion cloud chambers, shock tubes, and supersonic nozzles, because the TDCC is suitable for measuring small nucleation rates, for example, 10^{-4} to 10^{+2} drops/cm³/sec, while these other devices together typically extend the range of measured nucleation rates from (roughly) 10^3 to more than 10^{10} drops/cm³/sec. As a result, comparing nucleation rate data obtained from all these devices for the same working fluid makes it possible to obtain such data over quite wide ranges of rates, for example, ranges of 10^{12} to 10^{14} drops/cm³/sec are possible. This capability is of considerable utility and importance for the validation of models that attempt to describe the nucleation process.

Accurate measurement of nucleation (rates and critical supersaturation) by itself is significant, but the TDCC also has a number of other useful features. For example, the TDCC is self-cleaning, it operates continuously, nucleation is directly observable and measurable, and it can be operated over wide ranges of temperature and total pressure.¹ These features make the TDCC particularly amenable for unique and important applications. For example, in addition to accurate nucleation rate and critical supersaturation measurements, the TDCC has been used extensively to investigate photoinduced nucleation phenomena involving not only organic and inorganic vapors, but metal vapors as well;^{2,3} it has been used successfully to synthesize nanoscale particles;⁴ it has been used successfully for quantitative ion-induced nucleation investigations;⁵ it has been used to study polymerization kinetics;⁶ it has been used to examine unsteady (oscillatory or burst) nucleation;⁷ it has been used recently to model simultaneous nucleation and convection processes;^{8,9} and it is beginning to be used to investigate nucleation in the critical region.¹⁰

The importance of the TDCC to nucleation research is suggested further by the fact that nearly 50% of all nucleation rate and critical supersaturation data in the nucleation literature comes from diffusion-based devices such as the TDCC.¹¹ Indeed, much of the nucleation data currently in the literature describing condensation in unary and binary systems, photoinduced nucleation, and ion-induced nucleation can be traced to TDCC investigations. Further, these data are used often in the development of new and improved models of the nucleation process.^{12,13} Consequently, it is essential that all nucleation data derived from investigations using these devices be as reliable as possible. In fact, recent investigations from our laboratories have raised concerns regarding the reliability of a significant amount of nucleation literature data. The issue underlying this concern is directly related to our ability to model accurately the mass and energy transport processes occurring within the TDCC during operation. Recently, we have improved our understanding of the proper operation of the TDCC, and we have improved our description of these transport processes.^{8,14–17}

In this paper, we apply our model for transport in the TDCC to nucleation data obtained for butanol and pentanol vapors with helium as the background gas using the high-pressure cloud chamber (HPCC), which is a version of the TDCC specifically designed to allow operation over wide ranges of temperature and total pressure.^{1,18,19} We first present the detailed form of our model for mass and energy transport in the TDCC and then compare this to the simplified (1-D) model commonly used in the past to analyze TDCC nucleation data. Next, we compare results of nucleation experiments analyzed using each of these two models. Finally, we discuss the results of this comparison and the impact these results have upon the operation of the thermal diffusion cloud chamber.

Our intent in investigating the impact of convective transport and buoyancy-induced disturbances in the TDCC is not to reanalyze all of the data currently in the literature obtained using the TDCC. Rather, it is to examine select nucleation data, appropriate to the interests of the nucleation community, to determine the magnitude of this impact. By identifying the underlying reasons for and the potential extent of this effect,

[†] Part of the special issue "Howard Reiss Festschrift".

^{*} To whom correspondence should be addressed.

[‡] Catholic University of America.

[§] Manhattan College.

individual investigators can then decide whether it is warranted to review existing data and how best to do it if they deem it necessary.

Description of the Problem

There is an increasing body of evidence to indicate that the TDCC does not function precisely in the manner previously believed.^{20,21} For example, a large body of nucleation data obtained in our Nucleation Laboratory over the last several years clearly indicates that the onset of nucleation (as manifested by the calculated value of the critical supersaturation) is a (significant) function of the total pressure within the TDCC. As the total pressure increases, the nucleation rate is observed to decrease and, as a result, the calculated critical supersaturation increases. Further, this dependence has been shown to be a function of the temperature and the kind of background gas being used. We have reported this behavior extensively, and it has been confirmed in other laboratories, as well.^{1,18,19,22–25} There has been no such observation made when using expansion cloud chambers.²⁶ However, virtually all expansion cloud chamber data has been obtained at relatively low temperatures (typically less than ambient) and at low total pressures (typically below ambient). Further, on the basis of the conventional nucleation model and theoretical description of the nucleation process (or its several variants), there is little reason to expect the rather large effects that have been reported. However, some investigators have suggested there is reason to expect similar or smaller effects.^{27b,28}

As a result of the serious questions raised regarding these observations, as well as questions relating to the manner in which the HPCC was being operated, for example, wet versus dry walls, no wall heat, or small size,¹⁴ a detailed analysis of TDCC operation was carried out on the basis of a full two-dimensional model of transport within the chamber.^{14,15} The results of that analysis clearly suggested the possibility of buoyancy-driven convective instabilities being generated along the wall of the TDCC for both wet and dry wall operation. To avoid the effects of these disturbances entirely, the diameter to height (aspect) ratio of the TDCC design would have to exceed, by a considerable amount, values that are commonly being used.^{8,14}

Perhaps the most important result of that analysis was the ability to predict the value of the total pressure that would give rise to these instabilities so that one could determine a priori what values of total pressure to use to avoid generating such disturbances.¹⁵ The expression that relates this value of the limiting total pressure to TDCC operating conditions, for example, the upper plate temperature and type of working fluid and background gas, is

$$P_{\text{tot,lim}} = P_{\text{vap}}(T_U) \times \left(\frac{M_v}{M_g} - 1 \right) \times \left(\frac{B}{T_U} - 1 \right) \quad (1)$$

In eq 1, $P_{\text{tot,lim}}$ is the total pressure not to be exceeded to avoid generating buoyancy-driven disturbances along the wall for a given upper plate temperature, T_U , in Kelvin, P_{vap} is the equilibrium vapor pressure of the working fluid, M_v and M_g are the molecular weights of the working fluid vapor and background gas, respectively, and B is the constant from the Clausius–Clapeyron vapor pressure equation.

The existence of buoyancy-driven convective instabilities in the TDCC was later confirmed by a more comprehensive analysis that allowed for the existence of convective flow within

the TDCC.⁸ This analysis was later confirmed for the TDCC by other investigators.^{9,17}

As a result of these investigations, it has become clear that there is a need to carefully determine the extent to which convective transport, in general, plays a role in determining TDCC operating conditions. In particular, we need to know to what extent does convective transport contribute to the observed dependence of the critical supersaturation on total pressure, temperature, and background gas as described above. We have previously demonstrated that using the full two-dimensional model to describe transport in the TDCC results in different (lower) values for the calculated supersaturation (as compared to the one-dimensional results).^{8,17} What we need to determine is the extent to which this is true over the range of total pressures and temperatures used in our experiments, as well as conditions at lower temperatures and total pressures. Further, we need to determine better values to use for the aspect ratio when using current or designing future versions of the TDCC to minimize effects due to these disturbances and allow confident application of the simpler one-dimensional model to describe transport within the TDCC. The primary purpose of this paper is to provide a better understanding of these issues.

Summary Description of the Experiments

Much has been written describing construction and operation of the thermal diffusion cloud chamber, so it is unnecessary to repeat that level of detail here.^{20,21} We have presented in considerable detail the description of the HPCC and how it is used to make nucleation measurements.^{1,18} We have also described on numerous occasions the procedures used to make constant temperature and constant pressure nucleation measurements with the HPCC.^{19,22,23} In this paper, we present only a short summary introducing a few key dimensions and features to make clear the constraints imposed on the mathematical analysis and the physical meaning of the boundary conditions, especially the sidewall boundary conditions as these turn out to be important in the understanding of the role of convection in diffusion cloud chamber operation.

Essentially, the HPCC is composed of a quartz ring mounted with O-rings between two solid metal plates. The region between the two plates and enclosed by the ring is where nucleation occurs. The geometry of this working area is cylindrical. A shallow pool of working fluid is placed on the lower plate inside the chamber as a source of vapor. This shallow pool of liquid is heated from below. Thus, liquid vapor and the background gas occupy the region above the pool. During operation, the aspect (diameter to height) ratio of this HPCC is 7.5.

The quartz ring is 0.0152 m high with an outside diameter of 0.1581 m. It is 0.0272 m thick and has a tensile strength rated to withstand pressures up to 1.01×10^7 Pa. Both metal plates are 0.2032 m in diameter and 0.0244 m thick and are either OFHC copper or high strength copper–nickel alloys. The inside surface of each plate is polished to a smooth (glassy) finish. The inside surface of the top plate is machined with a bevel of 1 degree to promote draining of the condensate to the walls. O-rings provide a seal between the metal plates and quartz ring. The metal plates do not contact the quartz ring except through liquid (condensate at the top and the liquid pool at the bottom) that fills the small space (typically 2.5×10^{-5} to 1.3×10^{-4} m) between the metal and the quartz. This is an important point since it results in good thermal contact between the metal plates and the upper and lower edges of the quartz ring.

Temperatures are measured using four calibrated thermocouples: Two are embedded in the top plate just above the plate

surface, and two are sealed through the lower plate so their tips just dimple the surface of the working fluid. Total pressure is measured using a calibrated Heise pressure gauge connected to one of the access ports in the top plate. The background gas pressure is established using a high-pressure tank of high-purity helium (99.999%) obtained from Air Products.

All nucleation data used in the analysis presented here were obtained using the HPCC described above. The 1-butanol data were taken from ref 19 and the 1-pentanol data were taken from ref 23. All thermodynamic and hydrodynamic data necessary to solve the equations described below were taken from those references. Details of those experiments are available in these references.

Description of the Model

As we stated earlier, the goal of this work is to examine the effect buoyancy-induced convection can have on the computed supersaturations in the TDCC. To make this comparison, we examine data for pentanol and butanol taken at (essentially) constant nucleation temperature over a wide range of total pressure. Results of calculations of the critical supersaturation will be given using both the typical 1-D model describing the TDCC^{14,20} and the more realistic 2-D model, which accounts for the important effects of wall-induced buoyancy convection.^{8,16}

Typically, the temperature, mole fraction, density, and supersaturation conditions inside the TDCC are obtained by solving the 1-D balances on thermal energy and mass transport. It has been typical to solve these equations describing vapor and energy transport in molar units since it facilitates calculation of the supersaturation and can be done without direct reference to the velocities within the chamber. The underlying equations in the 2-D model described here are essentially the same, but since mass average velocities are needed for the momentum equation, the equations we present are cast using a mass basis rather than a molar basis.

We assume that the diffusive flux of the vapor component, A, through a background gas, B, consists of two components: a concentration induced, ordinary diffusion term, $\mathbf{j}_A^{(x)}$, and a second flux contribution induced by the thermal gradient that exists between the chamber plates (Soret effect), $\mathbf{j}_A^{(T)}$. Therefore, the total mass flux, \mathbf{j}_A , of the vapor component, A, is given by

$$\mathbf{j}_A = \mathbf{j}_A^{(x)} + \mathbf{j}_A^{(T)} = [-\rho D_{AB} \nabla w_A] + [-\rho D_{AB} \alpha_T w_A (1 - w_A) \nabla \ln T] \quad (2)$$

where ρ is the total density, D_{AB} is the binary diffusion coefficient, w_A is the mass fraction of component A, α_T is the thermal diffusion ratio, and T is the temperature. This diffusive flux of A in eq 2 is relative to the mass average velocity, u , of the system.

The total energy flux with respect to the mass average velocity of the system is composed of three terms: The typical conduction term, $\mathbf{q}^{(c)}$; a species interdiffusion term, $\mathbf{q}^{(d)}$; and the reciprocal to the Soret effect, the concentration-induced Dufour energy flux, $\mathbf{q}^{(s)}$. For the binary system, using the simplification that $\mathbf{j}_A = -\mathbf{j}_B$, these three terms are given by

$$\mathbf{q} = \mathbf{q}^{(c)} + \mathbf{q}^{(d)} + \mathbf{q}^{(s)} = [-k \nabla T] + [(h_A - h_B) \mathbf{j}_A] + \left[\alpha_T \frac{RTM^2}{M_A M_B} \times \mathbf{j}_A \right] \quad (3)$$

where k is the mixture thermal conductivity, h_i is the specific

enthalpy of component i , R is the ideal gas constant, and M_i and M are the molecular weights of component i and the mixture, respectively. If these energy and mass fluxes are assumed to be steady throughout the chamber, then by conservation we have

$$\nabla \cdot (\rho \mathbf{u} h) = -\nabla \cdot \mathbf{q} \quad (4)$$

and

$$\nabla \cdot (\rho \mathbf{u} w_A) = -\nabla \cdot \mathbf{j}_A \quad (5)$$

To solve for the velocity profiles and hence the convective contributions to the fluxes given in eqs 4 and 5, both the continuity equation and the momentum equation are needed. These equations are

$$\nabla \cdot (\rho \mathbf{u}) = 0 \quad (6)$$

and

$$\nabla \cdot (\rho \mathbf{u} \mathbf{u}) = -\nabla \cdot \boldsymbol{\tau} + \nabla P + \rho \mathbf{g} \quad (7)$$

respectively. In eq 7, P is the pressure, $\boldsymbol{\tau}$ is the stress tensor, and \mathbf{g} is the gravitational level. The stress tensor components for the system are given in detail in reference 8. Equations 4–7, coupled with an appropriate equation of state, can be used to calculate the temperature, concentration, and flow fields within the TDCC. These model equations are solved in 2-D with cylindrical coordinates using finite differences and the SIMPLER method.^{8,29}

Although we typically utilize more realistic equations of state, for example, Peng–Robinson, for TDCC investigations, we choose the ideal gas equation of state for this analysis in the interests of mathematical and computational expediency. All the 1-D and the 2-D model calculations described below were carried out using the ideal gas equation to allow meaningful comparison. The effect of using a real gas equation of state on the calculated TDCC operating conditions can be significant and has been addressed elsewhere.¹⁹ Using the ideal gas equation of state in this analysis affects the calculated supersaturations and nucleation temperatures only slightly as can be verified by comparing the calculated 1-D solutions shown below with those published elsewhere obtained utilizing the Peng–Robinson equation of state.^{19,23} The conclusions arising from our investigation are unaffected by our choice for the equation of state.

In the 1-D modeling of the chamber, the same contributions to the vapor and energy transport as noted by the terms in eqs 2 and 3 are considered, but the equations are written in molar rather than mass form. The equations for the molar vapor flux of A, N_{Az} , and energy flux, q , are

$$N_{Az} = -\frac{c D_{AB}}{1 - x_A} \left[\frac{dx_A}{dz} + \alpha_T x_A (1 - x_A) \frac{d \ln T}{dz} \right] \quad (8)$$

$$q = -k \frac{dT}{dz} + N_{Az} \bar{H} + N_{Az} \alpha_T RT (1 - x_A) \quad (9)$$

where c is the molar concentration, x_i is the mole fraction of component i , z is the axial spatial coordinate, and \bar{H} is the molar enthalpy. These flux equations are written with respect to stationary coordinates so they contain both the diffusive and convective (bulk axial flow) contributions to the fluxes. Again, as in the 2-D model, the concentration and temperature profiles can be calculated by assuming the fluxes are steady and constant.

One additional simplification made in the derivation of eqs 8 and 9 is that the flux of the background gas, N_{Bz} , is assumed

to be zero. Since it is assumed that there is no flux of the background gas into the upper or lower plate boundaries, the flux of the background gas throughout the chamber in the 1-D model must be zero by continuity. This same boundary condition is used for the 2-D model, but there is no restriction on the transport of the background gas within the chamber. Even though there is no net transport of the background gas through the chamber in the 2-D model, it is now possible to predict and describe recirculation of the background gas within the chamber.¹⁶

Chamber Geometry and Model Boundary Conditions

To present a meaningful comparison between these two models of the chamber, we will examine experimental measurements of the critical supersaturation with total pressure at constant nucleation temperature for 1-butanol and 1-pentanol. Both sets of data were obtained over a wide range of total pressure using the HPCC with helium as the background gas. Both sets of experiments were carried out using wet wall operation. Under these conditions, no wall heat was applied to the quartz ring so that vapor within the chamber was allowed to condense on the chamber sidewalls forming a thin transparent film of condensate that slowly and continuously drained from the upper to the lower plate. The magnitude and impact of this film flow has been examined in detail elsewhere.³⁰ The presence of this flow is ignored in this analysis, although it will need to be examined more carefully in the future with respect to the effect on the boundary conditions at the walls.

When applying the 1-D model, the internal dimensions of the chamber are not required, but they are necessary when applying the 2-D model. Furthermore, if buoyancy-driven convection is present, the magnitude of this convection will scale with the volume of the cloud chamber.⁸ This is an important, new piece of information to describe proper operation of the TDCC. In the past, the only concern about chamber size in designing and using the TDCC was to scale the size of the chamber by using the aspect ratio. We have observed for a number of years that the smaller cloud chambers seem to function more reliably. This is one of the reasons we adopted the smaller chamber for our use. The results of these 2-D studies confirm that there are good reasons why the smaller chambers should be more reliable.

A number of the boundary conditions used in the 2-D model are the same as those used in the 1-D model. At all boundaries (top, bottom, and sidewall), it is assumed that the vapor is in equilibrium with the condensed liquid at these surfaces. As for the temperature of the sidewall, we adopt the reasoning by Fisk et al. that the conduction between the lower and upper plates is the dominant transport mechanism so that, with unheated walls, there is a linear drop in temperature along the wall between these two boundaries.³¹ We shall return to this issue later.

Finally, boundary conditions are needed for the velocity components. For this model analysis, we assume that all tangential velocity components are zero.⁸ The normal velocity components follow from the assumption that there is no flux of the background gas at the computational boundaries. Therefore,

$$n_{B\zeta} = -\rho D_{AB} \frac{dw_A}{d\zeta} + \rho u = 0 \quad (10)$$

where n_B represents mass flux of the background gas and ζ represents the spatial component normal to the wall. It follows from this that the normal velocity component, u , at the wall is

Scr vs Ptot - PEOH/HE

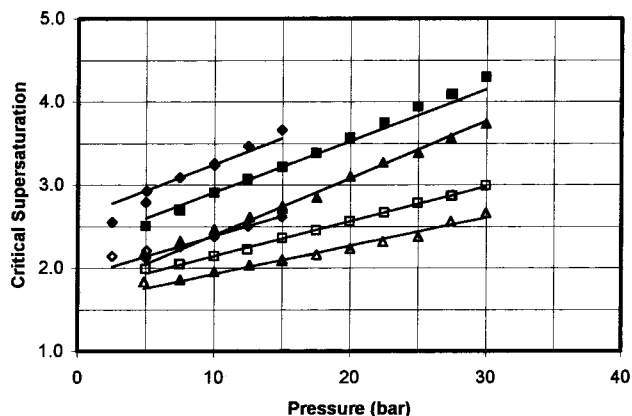


Figure 1. Variation of critical supersaturation of 1-pentanol with total pressure for the 1-D analysis (solid symbols) and the 2-D analysis (open symbols). The solid lines are regression fits to the linear portions of the data sets and are included to emphasize trends in the data. Nucleation temperatures: diamonds, 356 K; squares, 366 K; triangles, 377 K. See text for details.

$$u = \frac{D_{AB}}{1 - w_A} \frac{dw_A}{d\zeta} \quad (11)$$

Modeling Results

1-Pentanol. The 2-D model discussed above is able to account for buoyancy-induced convection, which is suspected to influence the maximum attainable supersaturation in the TDCC and result in differences between the 2-D calculated values and solutions calculated using the typical 1-D model. The emphasis of this work is to examine the magnitude of this effect on two particular systems. To clearly delineate the differences due to sidewall buoyancy effects, the same numerical model is used to calculate both the 2-D and 1-D results. This is achieved by setting the temperature, mass, and axial velocity gradients to zero at the chamber sidewall boundary, in essence eliminating any sidewall disturbances and possible buoyancy effects induced by them. Although this approach is more time-consuming from a computational standpoint, it ensures that errors due to grid refinement, physical properties, and so forth do not contribute to differences observed using the two models of the chamber.

Figure 1 is a plot of the calculated critical supersaturations for 1-pentanol in helium as a function of total pressure for both the 1-D and 2-D models at several nucleation temperatures. The 1-D results are denoted in the plot by the solid diamond, square, and triangle symbols while the 2-D results are shown as the corresponding open symbols. The solid lines included with each data set are linear regression fits to that data in each data set that fall within the stability boundaries of the HPCC operation.¹⁵ These lines are included to provide a visual aid to emphasize the linear portion of the dataset ranges. These lines are also included to help make evident the departure from linear behavior at the ends of the range of total pressure. As shown in the figure, there is an increase in the critical supersaturation with total pressure for each of the three isotherms for the 1-D model.

For the 2-D model, there is still an increase in the calculated critical supersaturation with total pressure, but the slope is smaller. Also, the calculated values of the critical supersaturation are smaller. The reduction in the critical supersaturation agrees (qualitatively) with results from Anisimov et al. for pentanol-helium.¹⁷ One other point in the 2-D model prediction is that there appears to be a subtle "leveling off" of the critical

supersaturation values at the lower end of the pressure scale. The lines included in the figure help to make this effect evident.

The pentanol data shown in Figure 1 were originally taken to show the effect of total pressure on the critical supersaturation at a constant nucleation temperature, and this nucleation temperature was obtained using the 1-D model. Therefore, there is some deviation in the calculated nucleation temperature for the data when using the 2-D model. Typically, this variation in nucleation temperature is in the range ± 1.5 K.

In the past, experimental results have shown that the calculated critical supersaturation depends on both the total pressure and the type of background gas. Although all of the 2-D results presented here are for helium as the background gas, an inference can be made regarding other background gases. The results obtained by applying the 2-D model to experimental data are plotted in Figure 1 and show a reduction in the calculated critical supersaturation (over that obtained using the 1-D model) with increasing total pressure. The 2-D analysis shows that this effect is due to convection induced by the presence of the sidewall as manifested in the boundary conditions. Since the magnitude of the convection will increase with increasing molecular weight of the background gas, it is expected that calculated critical supersaturations would be further reduced with higher molecular weight background gases such as argon or nitrogen.^{8,9} This is consistent with our experimental observations that the effect of total pressure on the calculated supersaturation increases with increasing molecular weight of the background gas.¹⁹

From this analysis, it is not clear if the dependence of critical supersaturation on total pressure that is evident in the 2-D results shown in Figure 1 is due to an intrinsic nucleation effect or if it is due to remaining inadequacies of our 2-D model in accounting for the reduction of the attainable supersaturation within the chamber because of wall-induced convection. For example, the actual sidewall boundary conditions are not as well known as the upper and lower plate conditions. Considering the simple model we used for these sidewall boundary conditions and the observed magnitude of the reduction in the calculated critical supersaturation, it may be possible that buoyancy-induced convection could be responsible for the remaining total pressure effect. In any case, further analysis and experiment will be needed to answer these questions.

1-Butanol. We analyzed existing butanol data obtained using the HPCC in the same manner described above for pentanol. The results of that analysis are shown in Figure 2 for both the 1-D and 2-D models. For butanol, the available data covers a larger range of total pressure. As in the pentanol case, the results from the 1-D model show an increase in the calculated critical supersaturation with total pressure. The solid lines in the figure were obtained in the same manner and included for the same reasons as described above for Figure 1. However, in the case of butanol, deviations from the linear portions of the data sets are more evident. This is especially true for the 348 K nucleation temperature data, which spans the largest pressure range. In this example, the data points in the lower pressure range are (essentially) linear in total pressure, but at higher pressures there is clearly curvature to the data points with total pressure. Similar behavior has been described in ref 27b. There appears to be a slight downward curvature of the data points at the lowest pressures in the 1-D dataset, although this effect is subtle.

The 2-D analysis of the data for butanol gives results similar to those obtained for pentanol. The calculated critical supersaturation of butanol still increases with total pressure at constant nucleation temperature, but the magnitude of the calculated

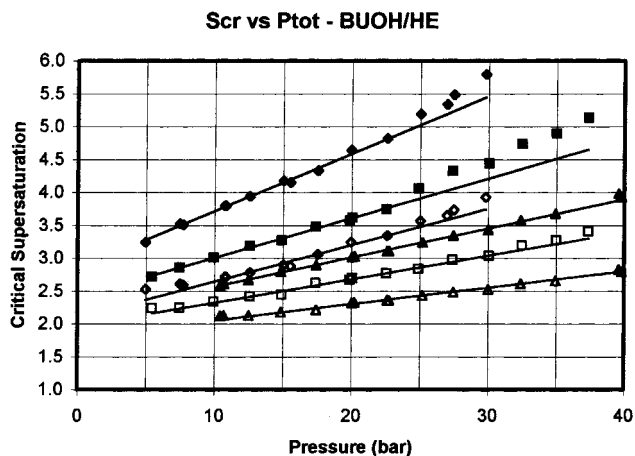


Figure 2. Variation of critical supersaturation of 1-butanol in helium with total pressure for the 1-D analysis (solid symbols) and the 2-D analysis (open symbols). The solid lines are regression fits to the linear portions of the data sets and are included to emphasize trends in the data. Nucleation temperatures: diamonds, 334 K; squares, 348 K; triangles, 363 K. See text for details.

supersaturations are significantly smaller, and the slope of the total pressure dependence is less than that obtained using the 1-D model. The variation of critical supersaturation with total pressure as determined using the 2-D model still exhibits the curvature evident in the 1-D representation of the data. This curvature is due to the onset of buoyancy-induced convection as described in our earlier efforts to model the total pressure dependence and is consistent with the stability boundary determined using eq 1.^{15,22,23}

For the butanol data, the leveling of the data at the lower pressures is more evident. If the observed pressure effect is due entirely to hydrodynamic processes within the chamber and not some pressure effect inherent in the nucleation process itself, then an accurate model of the chamber which accounts for convection should predict lines of constant supersaturation with pressure. As mentioned for pentanol, a relatively simple model for the chamber sidewall boundary conditions is used and it is expected that errors in such a model would increase with increasing convection and hence total pressure, consistent with the results shown in Figure 2. Further investigations are needed to verify whether this hypothesis is correct.

Conclusions

The thermal diffusion cloud chamber has been used extensively for nucleation measurements for more than three decades. In fact, much of the vapor to liquid critical supersaturation and nucleation rate data currently in the literature for unary and binary systems comes from such measurements. The TDCC is a unique, important tool for nucleation research, so it is critical that we understand exactly how the device actually functions to accurately determine operating conditions within the chamber. In the past, a reasonable one-dimensional model of the mass and vapor transport within the chamber was used to analyze operating conditions.^{20,21} Recently, it has become apparent that the one-dimensional nature of the model is inadequate to accurately describe TDCC operation especially under conditions associated with more novel applications of the device, for example, higher total pressures and nucleation temperatures.^{8,9,14-17}

We are working to resolve this problem by developing a full two-dimensional model of the diffusive and convective transport of mass and energy that not only accounts for buoyancy-driven convective flow but also accounts for the finite size of the

commonly used chambers. In this paper, we describe this two-dimensional model. In addition, we use the resulting equations to describe results of prior experiments dealing with the nucleation of 1-butanol and 1-pentanol vapors with helium as the background gas.

Results of this investigation clearly show that buoyancy-induced convective flows are an important part of TDCC operation. The role of the TDCC sidewall is fundamental in establishing these flows, and the effect of this additional mode of transport (additional to the usual axial diffusive flux) is to change the value of the calculated critical supersaturation and nucleation temperature in the regions of the TDCC where nucleation observations are made. In the cases of the butanol and pentanol vapors examined in this investigation, the effect is to reduce the value of the calculated critical supersaturation relative to that predicted using only the one-dimensional TDCC model. The effect upon the values of the nucleation temperature is smaller, for example, ± 1.5 K. Our results reported here are in general agreement with results from other investigators.¹⁷ Not only is the onset of convective instability at higher total pressures that we predicted earlier an important issue to consider for reliable chamber operation,^{15,22,23} but we find that other wall-induced flows, occurring over the range of total pressures, are also necessary to consider as well.

We mentioned that our decision for using the ideal gas equation of state in our analysis was based on convenience. The important conclusions we obtained were not affected by this choice because we treated both the 1-D and the 2-D cases the same. There are other refinements we have made to the more quantitative analysis of the TDCC that we also neglect here for convenience. For example, the solubility of the background gas in the liquid on the lower, upper, and sidewall surfaces has been ignored. In general, when we carry out nucleation measurements using the TDCC, we take these refinements into account.³²

It is important to point out that while our more careful modeling of the TDCC has resulted in a reduced total pressure effect on the calculated supersaturation (both slope and magnitude), this effect has not been eliminated. It may be that using more accurate sidewall boundary conditions will remove this dependence entirely, or it may be, as suggested by other investigators,^{27b,28} that there is, in fact, a pressure dependence on the nucleation of vapors not evident at ambient or lower total pressures. This remains to be determined by our future investigations.

We commented above on the importance of the sidewall boundary conditions to the reliable analysis of chamber operating conditions. In our analysis described above, we assumed a linear variation of wall temperature between the upper and lower chamber plates. In earlier work reported elsewhere, we assumed that the sidewall surface temperature would follow the temperature profile within the TDCC.^{8,15,16} As one might expect, these two profiles are not greatly different. However, if both are used to analyze critical supersaturation data and the results compared, we find that the differences in calculated supersaturations are generally about 5–10% with the latter approach having less of an impact on chamber conditions than the former. One might expect the actual variation of wall temperature with height to be somewhere between these two cases. In any event, the dependence of calculated critical supersaturation on total pressure does not go away using either of these two approaches.

The role of the sidewall temperature profile continues to be investigated.

Finally, we point out that it has become increasingly apparent that the sidewall of the TDCC needs to be as far as possible from the center of the chamber to minimize the effect of that wall on conditions at the center. It has always been believed that the aspect ratio needs to be maintained as large as convenient; however, as a result of this investigation and our other recent work,^{14,16,17} it is clear that common values for the aspect ratio, for example, 5–8, are probably not sufficient. Also, it has become clear that smaller chambers are less susceptible to buoyancy-induced convective disturbances. Since small chambers with large aspect ratios, for example, >10 , are somewhat difficult to work with, we also conclude that it is increasingly important that a full two-dimensional analysis of TDCC operation be employed whenever possible rather than rely on the approximate one-dimensional models.

References and Notes

- (1) See, for example, Heist, R. H.; Janjua, M.; Ahmed, J. *J. Phys. Chem.* **1994**, *98*, 4443 and references therein.
- (2) See, for example, He, H.; Heist, R. H. *J. Phys. Chem. A* **1997**, *101*, 9309 and references therein.
- (3) See, for example, Kalisky, O.; Heist, R. H. *J. Chem. Phys.* **1985**, *83*, 3668 and references therein.
- (4) See, for example, El-Shall, M. S.; Slack, W.; Vann, W.; Kane, D.; Hanley, D. *J. Phys. Chem.* **1994**, *98*, 3067.
- (5) See, for example, Kane, D.; Rusyniak, M.; Fisenko, S. P.; El-Shall, M. S. *J. Phys. Chem. A* **2000**, *104*, 4912 and references therein.
- (6) See, for example, Reiss, H. *Acc. Chem. Res.* **1997**, *30*, 297 and references therein.
- (7) See, for example, Heist, R. H.; Kacker, A.; Brito, J. *Chem. Eng. Commun.* **1984**, *28*, 117 and references therein.
- (8) Ferguson, F. T.; Nuth, J. A., III. *J. Chem. Phys.* **1999**, *111*, 8013.
- (9) Schaeffer, N.; Utheza, F.; Garnier, F.; Lauriat, G. *J. Chem. Phys.* **2000**, *113*, 8085.
- (10) Heist, R. H. unpublished data.
- (11) Heist, R. H.; He, H. *J. Phys. Chem. Ref. Data* **1994**, *23*, 781.
- (12) Dillmann, A.; Meier, G. E. A. *J. Chem. Phys.* **1991**, *94*, 3872 and references therein.
- (13) Girshick, S. L.; Chiu, C–P. *J. Chem. Phys.* **1990**, *93*, 1273.
- (14) Bertelsmann, A.; Heist, R. H. *J. Chem. Phys.* **1997**, *106*, 610.
- (15) Bertelsmann, A.; Heist, R. H. *J. Chem. Phys.* **1997**, *106*, 624.
- (16) Ferguson, F. T.; Heist, R. H.; Nuth, J. A., III. *J. Chem. Phys.* **2000**, *113*, 7398.
- (17) Anisimov, M. P.; Shandakov, S. D.; Polygalov, Yu. I.; Heist, R. H. *J. Chem. Phys.* **2001**, *114*, 899.
- (18) Heist, R. H.; Ahmed, J.; Janjua, M. *J. Phys. Chem.* **1995**, *99*, 375.
- (19) Bertelsmann, A.; Stuczynski, R.; Heist, R. H. *J. Phys. Chem.* **1996**, *100*, 9762.
- (20) Katz, J. L. *J. Chem. Phys.* **1970**, *52*, 4733.
- (21) Heist, R. H. In *Handbook for Heat and Mass Transfer Operations*; Cheremisinoff, N., Ed.; Gulf Publishing Co.: Houston, Texas, 1985; Vol. 1, Chapter 19.
- (22) Bertelsmann, A.; Heist, R. H. *J. Aerosol Sci.* **1998**, *28* (3), 259.
- (23) Bertelsmann, A.; Heist, R. H. *Atmos. Res.* **1998**, *46*, 195.
- (24) Chukanov, V. N.; Korobitsyn, B. A. *Russ. J. Phys. Chem.* **1989**, *63*, 1085.
- (25) Kane, D.; Fisenko, S. P.; Rusyniak, M.; El-Shall, M. S. *J. Chem. Phys.* **1999**, *111*, 8496.
- (26) Viisanen, Y.; Strey, R.; Reiss, H. *J. Chem. Phys.* **1993**, *99*, 4680.
- (27) (a) Itkin, A. L. *Aerosol Sci. Technol.* **2001**, *34* (6), 479. (b) Itkin, A. L. *Chem. Phys.* **2000**, *256* (1), 61.
- (28) Fisenko, S. P. private communication.
- (29) Patankar, S. *Numerical Heat Transfer and Fluid Flow*; Hemisphere: Washington, DC, 1980.
- (30) Bertelsmann, A. Ph.D. Thesis, University of Rochester, 1997.
- (31) Fisk, J. A.; Chakarov, V. M.; Katz, J. L. *J. Chem. Phys.* **1996**, *104*, 8657.
- (32) Chan, Y. F. MS Thesis, University of Rochester, 2001.